Disk Winds in Active Galactic Nuclei

James Chiang

NASA/GSFC, Code 661, Greenbelt MD 20771
and
Joint Center for Astrophysics/Physics Dept.,
University of Maryland Baltimore County, Baltimore MD 21250

* Norm Murray (Voit, Grossman) ← pre-1988
* Daniel Proga (Kallman, Stone, ...) ← Since then
· Nahum Arav, Dave Turnshek

MOTIVATION:

- ~10% of opt. selected RQQs have BALs in Lyα, CIV, NV, OVI, ... w/ $\Delta v_{BAL} \gtrsim 5000$ km s^{-1}
- ~15% of BAL QSOs have BALs in MgII, AlIII, ...
- large range of "detachment" velocities are seen $v_{detach} \approx 0$ to 10^4 km s^{-1}
- Aside from BALs, UV spectra of non-BAL & BAL QSOs are quite similar (Weymann et al 1991)
- P Cygni/O star analogy + unified model:

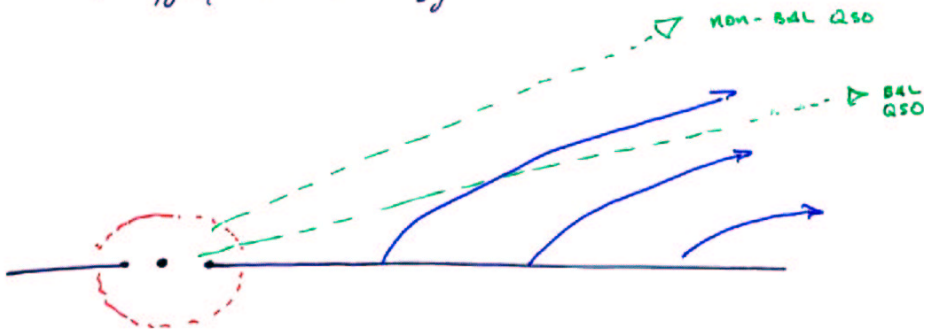

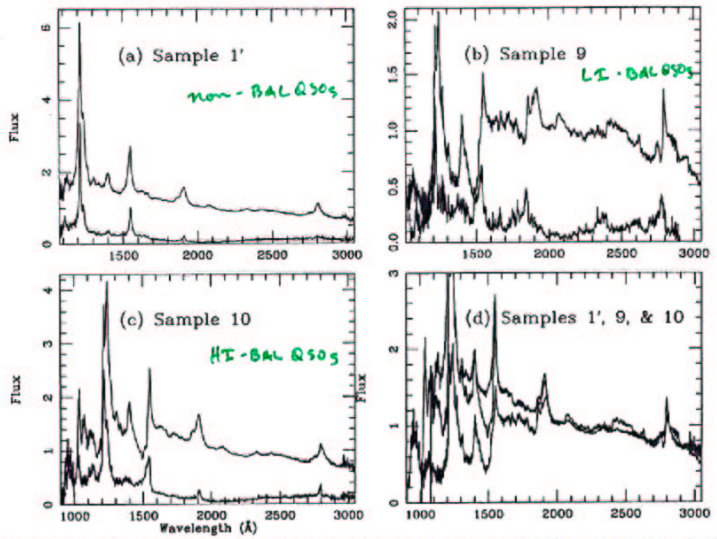

FIG. 3.—Panels *a*, *b*, and *c* are the averaged spectra and the associated rms values for samples 1' (the non–BALQSO sample), 9 (the Mg II–Al III BALQSOs), and 10 (the BALQSOs without noticeable Mg II or Al III absorption troughs), respectively. Panel *d* superposes the three averaged spectra, which have all been normalized to unity at about 2000 Å. Note that at the scale of panel *d* samples 1' and 10 are indistinguishable longward of the C IV absorption trough at about 1550 Å.

involves an unknown contribution from Fe II, is 34 Å for sample 1' and 38 Å for sample 10. Superposed on this broad component is a core. If we draw a flat effective continuum across the base of this core, the equivalent width of the core is 9 Å for both spectra and it has FWHMs of 3200 and 2800 km s^{-1} for the sample 1' and sample 10 spectra, respectively.

The region of the Al III–C III] lines is of special interest. Our individual measures and the accompanying K-S tests suggested some significant differences between the Al III in some samples, and weaker evidence for differences in C III]. We found no evidence from the K-S test for enhancement of the Al III/C III] ratio. Inspection of the spectra of Figure 3*d*, when plotted at a suitable scale, supports the evidence that there is some small enhancement of flux in the Al III–C III] region in the BALQSOs.

Instead, in Figure 4 we display the Al III–C III] region in a slightly different way. We take the difference between the BALQSO and non–BALQSO mean spectra and divide this difference by the fit to the continuum of the non–BALQSOs. The spectrum in Figure 4 can thus be interpreted as the difference in equivalent widths between the two samples.

Three things are noteworthy about Figure 4. First, the excess flux in the vicinity of the Al III–C III] blend is a broad feature which extends from about 1815 Å to about 1970 Å. Comparing it with the extent of the Al III–C III] emission in the sample 1' mean spectrum does suggest that Al III and C III] are involved, since these two features can be traced out to about these same wavelengths. On the other hand, there is no suggestion that the excess flux is a blend of two components, but it appears rather as a single smooth feature whose peak occurs at about 1895 Å. However, the signature of the blend is obvious in the two mean spectra from which this difference spectrum was formed, so that we have not blurred out the blend by the process of forming the two mean spectra. Moreover, there is an adjacent region of weaker but obvious excess flux extending from about 1700 to 1800 Å. These latter two properties argue that this excess flux is not due to Al III and C III] but may be due to Fe II or Fe III. The composite spectrum of Francis et al. (1991) clearly shows a broad complex of emission underlying the Al III–C III] blend.

Second, the region from 2000 Å to about 2650 Å in Figure 4 is remarkably flat, and the 2070 Å feature and broad Fe II complex from 2250 to 2650 Å have almost completely disappeared. If the excess flux discussed above is real and is due to Fe II, this suggests that some special excitation mechanism is at work which singles out the multiplets in the 1700–1970 Å region. In drawing the local continuum prior to deblending the Al III–C III], some of this excess was probably removed and what remained may have provided a greater percentage contribution to the Al III than to the C III].

Third, Figure 4 shows a *deficit* of flux increasing from about 1700 Å to the C IV emission line, shortward of which the BALQSO mean spectrum, and hence the difference spectrum, is dominated by the C IV absorption trough. This flux deficit could be an artifact in the construction of the two mean spectra, though we cannot think of any reason why this should

ACCELERATION MECHANISMS:

- Magneto-Centrifugal (Blandford & Payne 1982)
  - poloidal field anchored to disk, $\Omega \approx$ constant, $i > 30° \Rightarrow$ centrifugal accel.
  - Self-similar solutions (BP, et al);
    applied to BELR (Emmering, B. & Shlosman 1992; Bottorff et al (1997);
    BALR?
- Radiative Acceleration: $\dot{m} \sigma_{00} \approx \frac{L}{c}$ (σ_{00}: o.c. for BALS)
  - electron scattering, $\frac{L}{L_{Edd}} < 1$ (?)
  - dust, $T_{disk} > 2000$ K
  - bound-free (Chelouche & Netzer 2001)
  - → line driving ← (cf. Castor, Abbott & Klein 1975 (CAK) + others)

• line acceleration:

$$a_{rad} = \sum_{lines} \frac{\Delta\nu F_\nu}{c}\left(1 - e^{-\tau_{line}}\right)\frac{\kappa_{line}}{\tau_{line}} \qquad (\tau = \kappa\rho l)$$

($\Delta\nu \approx \frac{\nu}{c} v_{line}$)

• define optical depth parameter:

$$t \equiv \int \sigma_e \rho \, ds \qquad \text{static}$$

$$= \sigma_e \rho \, v_{th} \left|\frac{dr}{ds}\right|^{-1} \qquad \text{expanding}$$

(v_{th}: thickness of Sobolev surface)

$$\Rightarrow \quad a_{rad} = \left[\sum_{lines} \frac{\Delta\nu F_\nu}{F} \frac{1 - e^{-\kappa t/\sigma_e}}{t}\right]\frac{\sigma_e F}{c}$$

$$= M(t)\frac{\sigma_e F}{c}$$

($M(t)$: force multiplier)

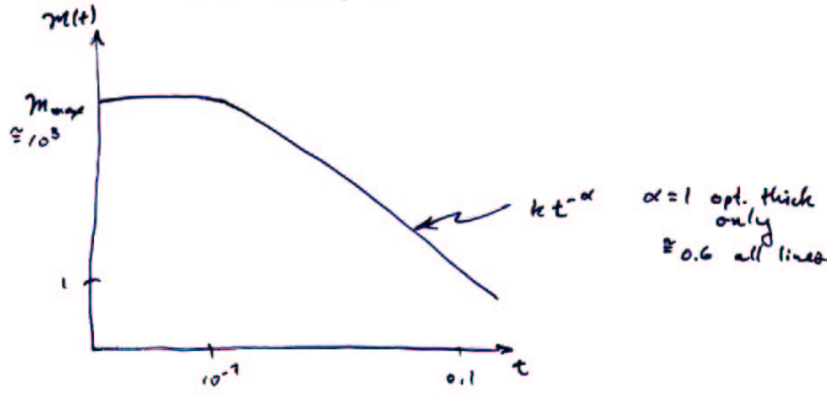

Ionization Constraints

- Ionization parameter

$$U \equiv \frac{\int_{\rm Ry}^{\infty} d\nu L_\nu/h\nu}{4\pi c r^2 n_H} \sim \frac{L(h\nu > {\rm Ry})}{4\pi r^2 n_H} \equiv \xi \qquad (8)$$

- In O-stars, $U \gtrsim 10^3$, but in AGNs require $U \lesssim 0.1$ for *bare* continuum in order to see lines and have radiative acceleration:

$$\left(\frac{U}{0.1}\right) \sim \left(\frac{L}{10^{46}{\rm erg\ s^{-1}}}\right)\left(\frac{R}{10^{17}{\rm cm}}\right)^{-2}\left(\frac{n_H}{10^{10}{\rm cm^{-3}}}\right)^{-1} \qquad (9)$$

- Solutions:
  - Place far from source (but for BELs in NGC 5548, $r_{BLR} \sim 10^{16}$ cm.)
  - High density $\Rightarrow$ small absorber size scale

$$l \sim \frac{N_{\rm abs}}{n_h} \lesssim 10^{13}\ {\rm cm} \qquad (10)$$

  $\Rightarrow$ small filling factors, $f \sim r/l \lesssim 10^{-4}$ and small, dense clouds with $T \sim 10^4$K

  $\Rightarrow$ Confinement problem: imbed clouds in hot gas, but require $T \sim 10^8$ K$> T_{\rm IC}$; or confine by magnetic pressure with $B \sim 1$ G (Rees 1987) $\Rightarrow$ magneto-centrifugal wind models (e.g., Emmering, Blandford, & Shlosman 1992; de Kool & Begelman 1995)

- Alternatively, one can filter out the ionizing flux:

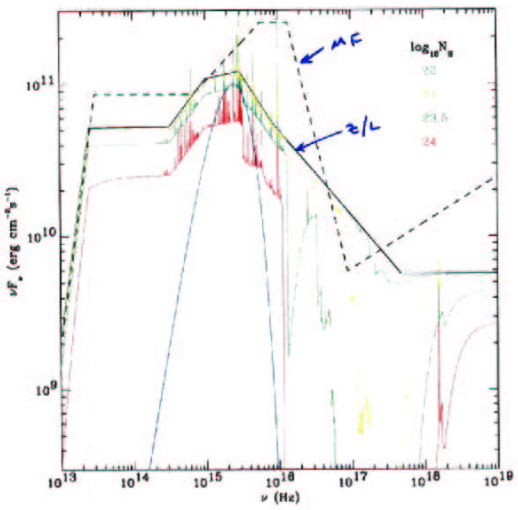

BAL QSOs are generally X-ray quiet and recent Chandra (Green et al. 2001) and ASCA (Mathur et al. 2000, 2001) results show that show that this is due to absorption with columns of $N_H \sim 10^{23}$–10^{24} cm^{-2}.

- Effect of X-ray absorption on force multiplier:

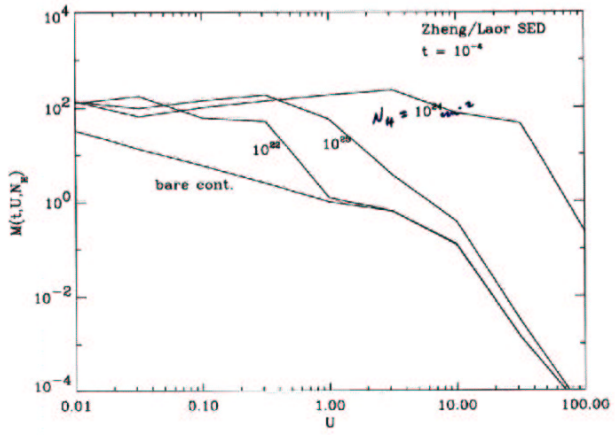

LINE DRIVEN DISK WIND (Murray et al 1995)

- radial equation (cf CAK)

$$v_r \frac{\partial v_r}{\partial r} = -\frac{GM}{r^2}\left[(1-\Gamma)\left(1-\frac{r_f}{r}\right) - \Gamma M(t)\right] - \frac{1}{\rho}\frac{\partial P_{gas}}{\partial r}$$

(centrifugal support)

$$v_r = v_\infty \left(1-\frac{r_f}{r}\right)^\beta \quad ; \quad v_\infty \approx \text{few} \times v_{esc}$$

$\beta = \frac{1+\alpha}{2-\alpha} \approx 1.3$ disk wind

$= 0.5$ O star

} v_r set by eff. gravity

- near wind footpoints

$$\frac{\partial v_r}{\partial r} \approx \frac{v_\infty}{r_f} \sim \frac{v_\infty}{r}$$ relevant for BEL

- $\dot{m} \approx 10^{26}\ g\ s^{-1}\left(M/10^8 M_\odot\right)(\Gamma)^{1/\alpha} \Rightarrow N_H \approx 10^{23}$–$10^{24}$ cm^{-2}

- Approximate solutions of r & θ equations $\Rightarrow$ 10% covering factor subject to $U_{max}=10$ at inner wind edge

- $M(t)$ computed using photoionization code, but had to posit $N_H \approx 10^{23}$ cm^{-2} filtering column ("hitchhiking gas", failed wind, disk atmosphere, ...)

$\Rightarrow$ require 2D hydro simulations

Disk Wind Broad Emission Lines

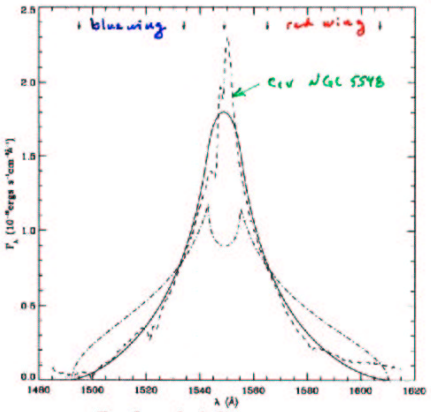

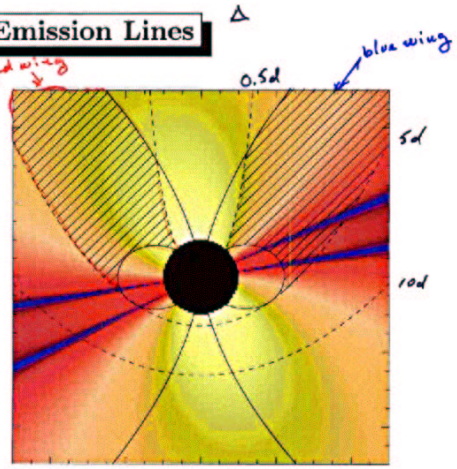

- Surface brightness:

$$F \sim S(r)\frac{1-e^{-\tau}}{\tau} \propto 1/\tau \quad (19)$$

$$\tau = \kappa\rho v_{\rm th}\left|\frac{dv}{ds}\right|^{-1} \quad (20)$$

- Velocity structure in line-driven disk wind verus Keplerian disk

$$\left|\frac{dv}{ds}\right| \simeq \sin^2 i\left(\frac{dv_r}{dr}\cos^2\phi + \frac{v_\phi}{r}\sin\phi\cos\phi\right) \quad (21)$$

$$v_r \simeq v_\infty(1-r_f/r)^\beta \qquad \beta \simeq 1.1\text{–}1.3 \quad (22)$$

$$\Rightarrow dv_r/dr \sim v_\infty r_f/r^2 \sim v_{\rm esc}/r_f \sim v_\phi/r_f \quad (23)$$

- Recover generic reverberation mapping response to continuum: red part of line leads blue part (NGC 5548, Fairall 9, 3C 390.3, NGC 4151,...)
- Smooth line profiles (Arav et al. 1997; 1998: $N_{\rm cloud} \gtrsim 10^7$)

NGC 4151

2.5D Simulations

(Proga, Stone, & Kallman 2000; PSK)

- Use ZEUS 2D code to integrate fluid equations
- Efficient quadrature scheme to compute radiation pressure forces

$$\vec{F}_{\rm rad}(\vec{r}) = \oint_\Omega \mathcal{M}(t)\left(\hat{n}\frac{\sigma_e I(\vec{r},\hat{n})}{c}d\Omega\right) \quad (15)$$

$$t = t(\hat{n}) = \frac{\sigma_e\rho v_{\rm th}}{|\hat{n}\cdot\Lambda\cdot\hat{n}|} \quad (16)$$

- Includes effects of ionization and shielding on line acceleration by positing an X-ray opacity:

$$\kappa_x = 40\ {\rm cm}^2\ {\rm g}^{-1} \qquad \xi < 10^5 \quad (17)$$

$$= 0.4\ {\rm cm}^2\ {\rm g}^{-1} \qquad \xi > 10^5 \quad (18)$$

where $\xi = e^{-\tau_x}\xi_{\rm bare}$, and uses the $\mathcal{M}(t,\xi)$ results of Stevens & Kallman (1990):

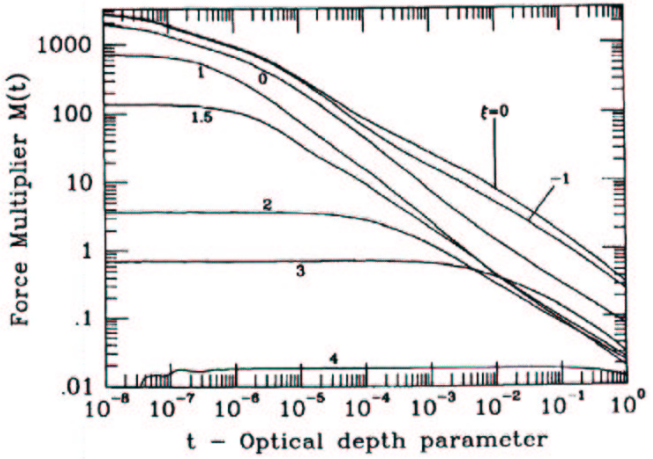

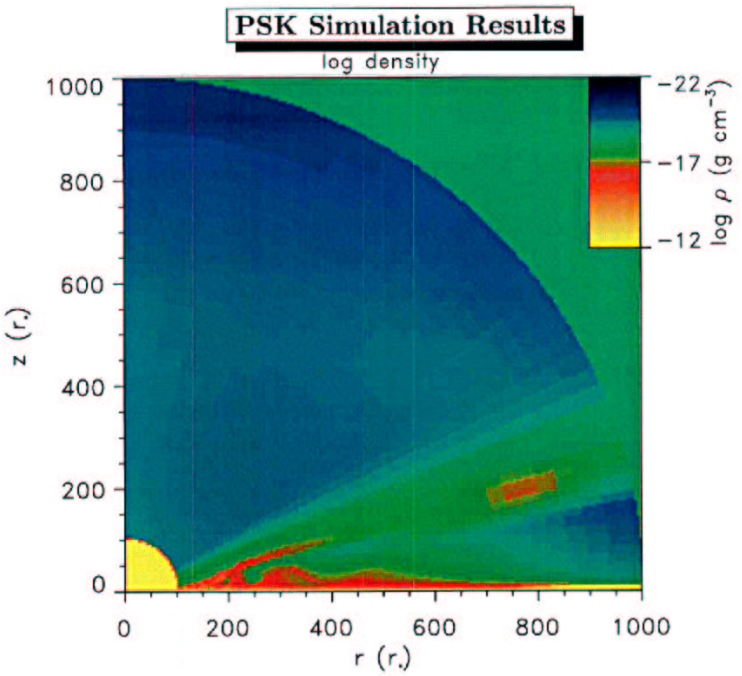

- High densities at wind innermost footpoints permit line driving even at inner edge until $\xi \gtrsim 10^2$.
- "Failed" wind at inner radius of $r_{\rm min} \sim 10^{16}$ cm (i.e., material which fails to achieve $v > v_{\rm esc}$ before $\xi > 10^2$) provides shielding from X-rays for streamlines at larger radii.
- Mass loss rates of $\dot{M} \sim 0.5\ {\rm M}_\odot\ {\rm yr}^{-1}$ for $\Gamma = 0.5$ and $M = 10^8\ {\rm M}_\odot$
- Material driven vertically from disk until it encounters upper surface.
- Bulk of $\dot{M}$ in uppermost streamlines (cf. Elvis 2000).

- Episodic events with $\mathcal{O}(10^2)$ density constrasts. ~~May be related to partitioning of luminosity: $L_{\rm disk} = \Gamma L_{\rm Edd} = L_* = 2L_{*,UV} = 2L_{*,X}$ (cf. Proga, Drew, & Stone 1998, 1999)~~
- Importance of L_{UV}/L_X (Proga 2001):

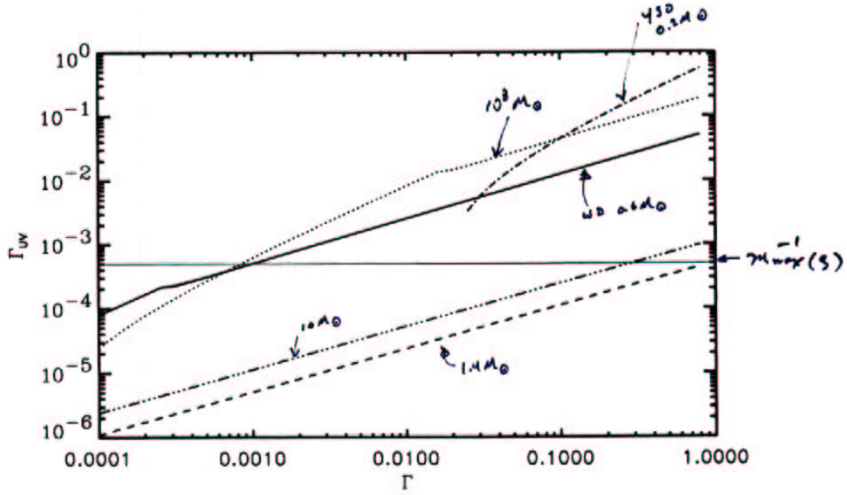

Conclusions (so far)

- Poloidal outflows will (likely) be driven from the UV emitting regions of disks (Proga 2001)
  high f near footpoints $\Rightarrow$ $v_{base} < 10$
- "Failed" wind at inner radii can provide needed X-ray shielding to allow $v_\infty > v_{esc}$ if $\kappa_X \gg \sigma_e$
  next step: self-consistent X-ray opacities
- Vertical velocity gradients $\Rightarrow$ single-peaked emission lines

$$\frac{dv_z}{dz} \sim \frac{\dot{v}_z}{v_z} \; ; \; \dot{v}_z \sim \frac{GMz}{r^3} \sim \frac{v_\phi^2}{r^2} z$$

$$v_z \sim v_{th} \sim v_\phi \frac{z}{r}$$

$$\Rightarrow \frac{dv_z}{dz} \sim \frac{v_\phi}{r} \checkmark$$

- Disk-wind BELR:
  - reverberation mapping ests of M_{BH}
    $\frac{\Delta M}{M} \lesssim 1$
  - Photoionization models & AGN SEDs:
    disk BELR + anisotropy of soft X-rays (at 54eV)
    $\Rightarrow$ large HeII EWs
    + Zheng/Laor instead of Matthews-Farland SED.

Disk Wind Connection to Broad Absorption Lines

- Time scales: *Location* of BAL absorption features stable over $t_{BAL} \gtrsim 10$ years, although depths do change (Barlow, Junkkarinen, & Burbidge 1989) $\Rightarrow r \gtrsim t_{BAL} v_r \sim (10^{8.5}\,\mathrm{s})(10^9\,\mathrm{cm\,s^{-1}}) \sim 10^{18}\mathrm{cm}$
- Complex trough structure:

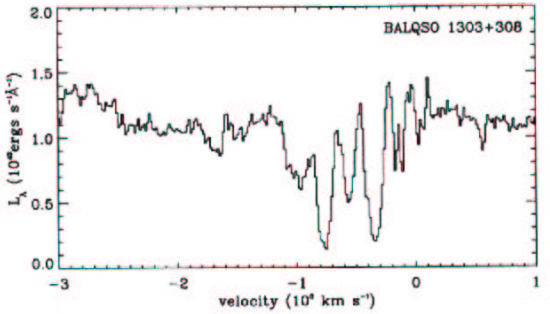

Streamline "sheets" with azimuthal symmetry (Arav et al. 1998):

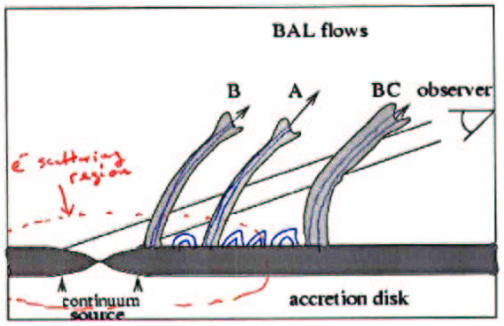

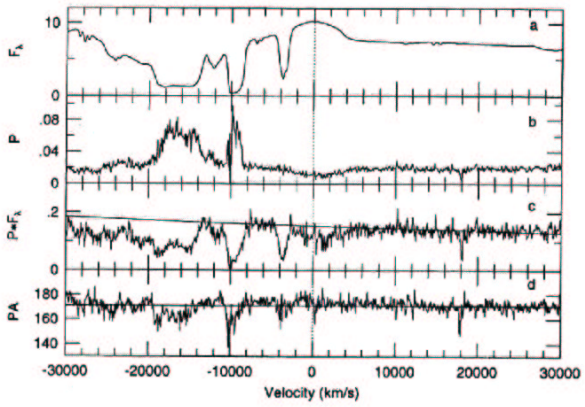

Figure 4. C IV trough of 0226−1024 ($z = 2.246$). (a) Total flux. (b) Fractional polarization. (c) Polarized flux with power law fit to the continuum. (d) Position angle. The mean continuum PA is 171°.

ates outward, then the higher velocity gas covers a larger portion of the electron scattering region, leading to lower polarization (for a given trough depth) at high velocities.

The sub-troughs also show PA rotations of up to −15° (Fig. 4), which are correlated to their velocity structure in polarized flux. This is naturally explained if the flow crosses the line of sight at an angle to the axis of the scattering region (Fig. 5b). Note that the rotations in the troughs are opposite to the rotation due to resonance scattering in the BALR, allowing a distinction between the two effects. This is expected since BALR streamers crossing the line of sight absorb polarized light at the same PA that they scatter light from the central continuum source. The PA in the troughs is driven away from the PA of the obscured electron scattered light.

Another striking detail in the spectropolarimetry of 0226−1024 is the absence of a polarization increase in the lowest velocity trough (Fig. 4). This suggests that it covers the electron scattering region almost completely. Perhaps it is due to BAL gas at a different radius or a completely different class of associated absorber. This is supported by the Keck HIRES data of T. Barlow and V. Junkkarinen (priv. comm.), which show that this trough breaks up into a number of sub-troughs at high resolution, whereas the other troughs remain smooth.

5.

B
e
a
l
t
p
s
t
r
a
o
s

R

A
B

C

K

T

W

$\frac{L}{L_{Edd}} \overset{?}{>} 1$

- BEL - BAL QSO similarities (Weymann et al 1991)

+ • relatively high incidence of BAL QSOs among brightest optically-selected QSOs; $N_H \sim 10^{23} - 10^{24}\ cm^{-2}$

+ • Boroson (2002):

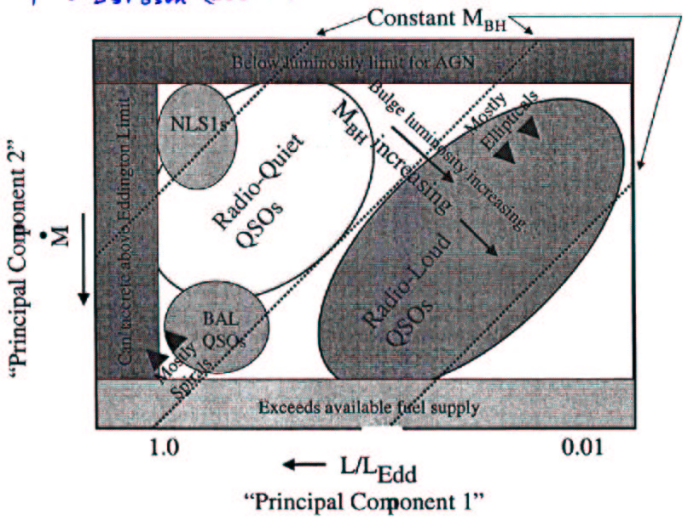

Fig. 7.— Interpretive diagram showing how PC1-PC2 plane provides basis for classification of AGNs.

+ $\frac{L}{L_{Edd}} > 1$ => DISK BELR !